EDGE ARTICLE

Light-induced decarboxylation in a photo-responsive iron-containing complex based on polyoxometalate and oxalato ligands†

Yan Duan,[a] João C. Waerenborgh,[b] Juan M. Clemente-Juan,[a] Carlos Giménez-Saiz*[a] and Eugenio Coronado*[a]

A new photoresponsive molecular polyanion in which two Fe(III) ions are simultaneously coordinated by two $[A-\alpha-PW_9O_{34}]^{9-}$ polyoxometalate units and two oxalato ligands has been obtained. When irradiated with UV light its potassium salt, **1**, exhibits a remarkable photocoloration effect, attributable to the partial reduction of the POM units to give rise to a mixed-valence species. The photoinduced process is intramolecular and involves electron transfer from the oxalato ligands, which partially decompose releasing CO_2, towards the Fe(III) and the POM. This mechanism has been confirmed by DRS, IR, XPS and Mössbauer spectroscopy, magnetism and elemental analysis. An analogous derivative of **1** containing malonato ligands does not exhibit such photoactive behaviour, which is evidence that the oxalate ligand is essential for the photoactivity of **1**. To our knowledge, **1** represents the first POM-based compound in which the photocoloration effect does not require the presence of intermolecular short interactions.

Introduction

The study of molecular-based materials whose physical or chemical properties can be tuned by applying external stimuli is attracting considerable interest in chemistry owing to the wide variety of functional materials that one can design.[1] As an external stimulus, light has been extensively used in this context. Thus, many examples of photomagnetic materials,[2] photochromic materials,[3] and electrochromic materials[4] have been reported.

Polyoxometalates (POMs) are metal–oxo clusters with W, Mo or V in their highest oxidation states which have the ability to accept, step by step, one or more electrons giving rise to mixed-valence coloured species (heteropoly blues or heteropoly browns).[5] POMs are being increasingly used as building blocks for the construction of systems with stimuli-responsive behaviour (in particular photoresponsive).[6] A common strategy is the combination of POMs with photosensitive groups in order to integrate the smart response in hybrid systems by means of electrostatic interactions, H-bonding, or other intermolecular

interactions. Recent examples include photoresponsive systems obtained by combining POM anions with azobenzene-modified cationic surfactants which can reversibly assemble and disassemble in solution with light irradiation,[6c] or supramolecular systems, obtained by using ionic liquids H-bonded to the surface of fluorescent POMs, that exhibit tunable photoluminescence properties by adjusting the pH of the solution.[6g]

Regarding the solid state, photochromic materials with strong UV-induced colour changes and remarkable coloration contrast can be obtained associating POM anions with organic cations (mainly organoammonium cations (OACs)).[6a,b,7] The photoactivity of such systems has been described in terms of a UV-induced photoreduction of the POM, concomitant with an intermolecular electron transfer assisted by proton transfer from the OAC towards the POM (Scheme 1). The effect is reversible in contact with air due to oxidation.

According to this mechanism, the photoactivity in these systems requires the formation of direct H-bonds between POMs and OACs, something that cannot be systematically achieved.[8] A way to improve the possibility of H-bond formation has been developed by P. Mialane, R. Dessapt *et al.*, consisting of directly grafting OAC-functionalized bisphosphonate ligands to the inorganic core of POMs.[6d] The same researchers also proposed a new class of solid-state photochromic hybrids combining sulfonium cations with POMs and so circumvented the dependence on an H-bonding network.[6e] In this case, the mechanism of the photochromic effect requires the establishment of short S···O contacts to allow UV-induced electron transfer from the sulfonium cations to the adjacent POM

[a]Instituto de Ciencia Molecular (ICMol), Universitat de València, c/Catedrático José Beltrán, 2, 46980 Paterna, Spain. E-mail: carlos.gimenez@uv.es; eugenio.coronado@uv.es

[b]Centro de Ciências e Tecnologias Nucleares, Instituto Superior Técnico, Universidade de Lisboa, 2695-066 Bobadela LRS, Portugal

† Electronic supplementary information (ESI) available: IR spectra, thermogravimetric analysis, X-ray crystallography, bond valence calculations, X-ray powder diffraction, UV-vis spectra of **1** and **2** in aqueous solution, coloration kinetics, Mössbauer spectroscopy and magnetic properties. ICSD reference 430800.
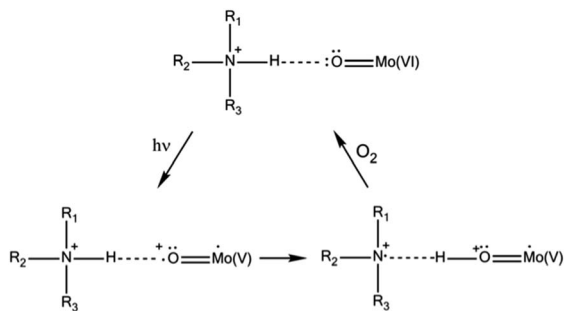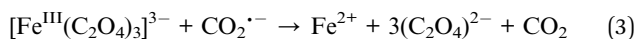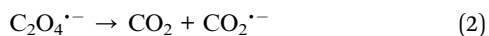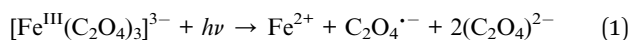
Scheme 1
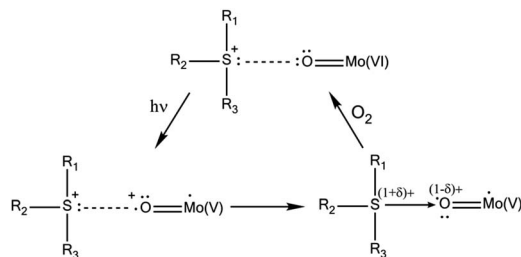
Scheme 2

(Scheme 2). As before, slow bleaching happens in contact with air.

On the other hand, some Fe(III) carboxylate complexes exhibit sensitivity to visible and UV light, which makes them photoreactive through ligand to metal charge transfer (LMCT) reactions and, therefore, valuable in the chemistry of environmental systems[9] and for laboratory photochemical applications in general (*e.g.* actinometry).[10] A prototypical example of such complexes is the tris(oxalato)ferrate(III) complex whose photoinduced LMCT reaction (reaction (1)) gives rise to the (photo)generation of Fe(II) ions (both in solution and in the solid state), and to a subsequent reductive reaction *via* $CO_2^{\bullet-}$ radical anions (reaction (3)).[11]

$$[Fe^{III}(C_2O_4)_3]^{3-} + h\nu \rightarrow Fe^{2+} + C_2O_4^{\bullet-} + 2(C_2O_4)^{2-} \quad (1)$$

$$C_2O_4^{\bullet-} \rightarrow CO_2 + CO_2^{\bullet-} \quad (2)$$

$$[Fe^{III}(C_2O_4)_3]^{3-} + CO_2^{\bullet-} \rightarrow Fe^{2+} + 3(C_2O_4)^{2-} + CO_2 \quad (3)$$

In this context, we are exploring the possibility of combining Fe(III) carboxylate complexes with POMs in the same molecular unit with the aim of obtaining a new type of photoactive solid state systems which would be independent of the establishment of any kind of inter- or intramolecular short interactions (*i.e.* H-bonds or S···O contacts). This can be realized if both carboxylate and POM act as ligands of a heteroleptic Fe(III) complex.

However, as far as we know, the only reported examples of Fe(III) complexes containing both oxalato and POM ligands are given by the family $[Fe_4(C_2O_4)_4(H_2O)_2(B-\beta-XW_9O_{33})_2]^{14-}$ (X = As[III], Sb[III], Bi[III]), although no photoactivity has been reported for these

compounds.[12] We report here the synthesis and characterization (X-ray crystal structure, diffuse reflectance, IR evolution upon irradiation, UV in aqueous solution, XPS, Mössbauer spectroscopy, and magnetic properties) of a novel mixed ferrioxalate–POM compound formulated as $K_{15}\{K \subset [[A-\alpha-PW_9O_{34})_2Fe_2(C_2O_4)_2]\} \cdot 29H_2O$ (**1**) which exhibits fast and evident photocoloration when exposed to direct sunlight or UV irradiation in the solid state. For comparison, we also report the analogous malonate derivative, $K_{15}\{K \subset [(A-\alpha-PW_9O_{34})_2Fe_2(C_3H_2O_4)_2]\} \cdot 27H_2O$ (**2**), which does not exhibit such photoactive behaviour, which is evidence that the oxalate ligand is essential for the photoactivity of **1**. We will demonstrate that the photocoloration process involves a simultaneous intramolecular electron transfer from the oxalato ligand to Fe(III) (leading to Fe(II)) and to the POM framework (leading to a reduced mixed-valence species containing W(v)). Such a process is accompanied by the release of CO_2.

Experimental section

General methods and materials

[57]Fe was obtained from CHEMGAS as iron powder with an isotope purity of 96.28% in [57]Fe. All other reagents were of high purity grade, obtained from commercial sources, and used without any further purification. The trivacant ligand $K_9[A-\alpha-PW_9O_{34}] \cdot 16H_2O$ was prepared according to a literature procedure[13] and confirmed by IR spectra. The potassium salts of the tris(oxalato)ferrate(III) and tris(malonato)ferrate(III) anions, $K_3[Fe(C_2O_4)_3] \cdot 3H_2O$ and $K_3[Fe(C_3H_2O_4)_3] \cdot H_2O$, were synthesized according to published procedures.[14] Pure water ($\rho > 18$ MΩ cm) was used throughout. It was obtained using an Elix-3/Millipore-Q Academic water purification system. IR spectra were recorded with KBr pellets on a Thermo NICOLET-5700 FT-IR spectrophotometer. Microanalysis was carried out with a Philips XL-30 scanning electron microscope coupled with a Philips EDAX Microanalysis system and the carbon content was determined by microanalytical procedures using an EA 1110 CHNS-O elemental analyser from CE Instruments. Thermogravimetric analysis was performed on a Mettler Toledo TGA/SDTA851e analyzer.

Diffuse Reflectance Spectroscopy (DRS) of solid samples was performed at room temperature and the data converted to obtain absorption spectra. DRS was carried out on a Jasco V-670 spectrophotometer equipped with an integrated sphere coated with $BaSO_4$ and an internal diameter of 60 mm, where the baseline was recorded using a poly(tetrafluoroethylene) reference. X-ray Photoelectron Spectroscopy (XPS) was performed at the X-ray Spectroscopy Service at the Universidad de Alicante using a K-Alpha X-ray photoelectron spectrometer system (Thermo Scientific). All spectra were collected using Al Kα radiation (1486.6 eV), monochromatized by a twin crystal monochromator, yielding a focused X-ray spot (elliptical in shape with a major axis length of 400 μm) at 3 mA C and 12 kV. The alpha hemispherical analyser was operated in the constant energy mode with survey scan pass energies of 200 eV to measure the whole energy band and 50 eV in a narrow scan to selectively measure particular elements. XPS data were analysed using Avantage software. A smart background function was used to approximate the experimental backgrounds. Charge

compensation was achieved with the system flood gun that provides low energy electrons and low energy argon ions from a single source.

Synthesis of $K_{15}\{K \subset [(A-\alpha-PW_9O_{34})_2Fe_2(C_2O_4)_2]\} \cdot 29H_2O$ (1). $K_3[Fe(C_2O_4)_3] \cdot 3H_2O$ (0.178 g, 0.363 mmol) was dissolved in 3 mL of milli-Q water at 60 °C under stirring. To this emerald green solution, solid $K_9[A-\alpha-PW_9O_{34}] \cdot 16H_2O$ (0.387 g, 0.135 mmol) was added in small portions. By the end of the addition the colour of the solution changed from emerald green to olive green. The solution was filtered while hot and the filtrate kept in the dark at room temperature in an open vial. After two hours, needle-shaped, light yellowish-green crystals were formed which were filtered and washed with milli-Q water to afford 0.251 g of the pure product (63% based on $[A-\alpha-PW_9O_{34}]^{9-}$).

Selected IR bands (2% KBr pellet 2500–400 cm^{-1}) (Fig. S1†): 1664.6(m), 1654.8(m), 1637.4(m), 1618.5(m), 1401.0(s), 1284.9(s), 1076.4(m), 1019.8(s), 940.9(m, sh), 885.2(w), 854.5(w), 741.5(m, sh), 658.8(s), 595.3(w), 518.4(m). Anal. calcd (found) for $K_{15}\{K \subset [(A-\alpha-PW_9O_{34})_2Fe_2(C_2O_4)_2]\} \cdot 29H_2O$: C 0.82 (0.81), Fe 1.90 (1.90), P 1.05 (0.90), W 56.35 (56.85), and K 10.61 (10.24). The TGA curve of **1** (Fig. S2†) shows two distinct weight loss steps (the first one from 25 to *ca.* 203 °C and the second one from 203 to *ca.* 450 °C, with a total weight loss of 10.57%), which correspond mainly to the loss of crystal waters and to the decomposition of the oxalato ligands, respectively (calcd 10.56%, see the ESI†).

Synthesis of $K_{15}\{K \subset [(A-\alpha-PW_9O_{34})_2Fe_2(C_3H_2O_4)_2]\} \cdot 27H_2O$ (2). The synthesis of **2** was carried out following the same procedure as for **1**, except that different amounts of the starting materials were used: 0.970 g (1.95 mmol) of $K_3[Fe(C_3H_2O_4)_3] \cdot H_2O$ (dissolved in 15 mL of water) and 1.935 g (0.67 mmol) of $K_9[A-\alpha-PW_9O_{34}] \cdot 16H_2O$. Light green crystals (1.670 g in the first crop) were collected after one night, washed with a small amount of cold water and dried in air (yield: 85% based on $[A-\alpha-PW_9O_{34}]^{9-}$).

Selected IR bands (2% KBr pellet 2500–400 cm^{-1}) (Fig. S1†): 2361.8(m), 1598.2(m), 1424.6(s), 1384.4(s), 1074.6(s), 1016.2(s), 937.0(s), 846.3(s), 742.4(m, sh), 666.5(s), 515.2(w). Anal. calcd (found) for $K_{15}\{K \subset [(A-\alpha-PW_9O_{34})_2Fe_2(C_3H_2O_4)_2]\} \cdot 27H_2O$: C 1.22 (1.18), Fe 1.90 (1.91), P 1.05 (0.98), W 56.25 (57.80), and K 10.60 (10.03). The TGA curve of **2** (Fig. S3†) shows three distinct weight loss steps. The first step (25–203 °C) is attributed to the loss of water molecules. The second (203–350 °C) and third steps (350–450 °C) correspond to the decomposition of the malonato ligands. After that, no significant weight loss is detected. The total weight loss observed is 10.66% (calcd 10.44%, see the ESI†).

Synthesis of $K_{15}\{K \subset [(A-\alpha-PW_9O_{34})_2{}^{57}Fe_2(C_2O_4)_2]\} \cdot 29H_2O$ ($1-^{57}Fe$) and $K_{15}\{K \subset [(A-\alpha-PW_9O_{34})_2{}^{57}Fe_2(C_3H_2O_4)_2]\} \cdot 27H_2O$ ($2-^{57}Fe$). $1-^{57}Fe$ and $2-^{57}Fe$ were obtained following the same procedures as for **1** and **2**, but using $K_3[{}^{57}Fe(C_2O_4)_3] \cdot 3H_2O$ and $K_3[{}^{57}Fe(C_3H_2O_4)_3] \cdot H_2O$ as starting materials, respectively. These ^{57}Fe enriched tris(carboxylate)ferrate(III) salts were obtained as follows. Solid ^{57}Fe (0.10 g, 1.79 mmol) and 5 mL of concentrated hydrochloric acid (12.1 mol L^{-1}) were mixed and heated to 60 °C with stirring for one hour. Then, 5 mL of 30% H_2O_2 was added and the resulting clear, yellowish-green

solution was rotavaporated several times with water to remove residual H_2O_2, until yellow crystals were obtained ($^{57}FeCl_3 \cdot 6H_2O$). The crystals were dissolved in 2 mL of water and a solution containing KOH (0.451 g, 8.05 mmol) and oxalic acid (0.506 g, 5.62 mmol) in 5 mL of water was added. The mixture was allowed to evaporate slowly at room temperature and, after several days, 0.72 g of green crystals of $K_3[{}^{57}Fe(C_2O_4)_3] \cdot 3H_2O$ was obtained (yield: 82.1% based on ^{57}Fe). $K_3[{}^{57}Fe(C_3H_2O_4)_3] \cdot H_2O$ was obtained using the same procedure but with replacing oxalic acid by malonic acid (yield: 94.0% based on ^{57}Fe).

Preparation of irradiated samples of 1. The samples were irradiated with two (for the DRS and IR measurements) and ten (for elemental analysis, TGA and XPS measurements) Luzchem LZC-UVA lamps ($\lambda_{exc} = 351$ nm, $P = 8$ W), and for Mössbauer spectroscopy with one Spectroline, Model ENF-260c/FE, UV lamp ($\lambda_{exc} = 365$ nm). Anal. calcd for a 3 day irradiated sample of **1** under vacuum: C (0.49). The TGA curve (Fig. S4†) shows two distinct weight loss steps (the first one from 25 to *ca.* 203 °C and the second one from 203 to *ca.* 450 °C, with a total weight loss of 7.57%), which correspond mainly to the loss of crystal waters and to the decomposition of oxalato ligands, respectively. From the elemental analysis and TGA results, a formula of the irradiated compound can be written as $K_{16}[(PW_9O_{34})_2Fe_2(C_2O_4)_{1.16}] \cdot 20.6H_2O$.

X-ray crystallography. Suitable crystals of **1** and **2** were coated with Paratone N oil, suspended on small fibre loops, and placed in a stream of cooled nitrogen (120 K) on an Oxford Diffraction Supernova diffractometer equipped with a graphite-monochromated Enhance (Mo) X-ray source ($\lambda = 0.71073$ Å). The data collection routines, unit cell refinements, and data processing were carried out using the CrysAlis software package[15] and structure solution and refinement was carried out using SHELXS-97 and SHELXL-2014.[16] All atoms were refined anisotropically in both crystal structures except some water molecules of solvation which had partial occupancies. An analytical numeric absorption correction was applied to the data of **1** using a multifaceted crystal model[17] integrated in the CrysAlis program, while for **2** a multi-scan absorption correction based on equivalent reflections was applied to the data using the program SORTAV.[18] In case of **1**, many residual densities were found in the final Fourier maps near the heavy W or Fe atoms. These residuals are attributed to relatively small twin components, which account for less than 10% of the main component and, therefore, were left unmodelled. In **2** residual densities are found near the water molecules of crystallization located in the regions between the large polyoxometalates. These regions are usually occupied by disordered water molecules and metal cations. The hydrogen atoms of the malonato ligand were included at the calculated positions and refined with a riding model. The hydrogen atoms of water molecules were not located. Crystallographic data for the two structures are summarized in Table S1† and Fe–O bond distances and O–Fe–O angles are shown in Table S2.†

Mössbauer spectroscopy. Due to the low Fe content of **1** and **2** and the presence of W, which strongly absorbs the 14.4 keV Mössbauer gamma rays, the samples for Mössbauer spectroscopy were prepared using ^{57}Fe enriched starting material. The

spectra were collected at room temperature in transmission mode using a conventional constant-acceleration spectrometer and a 25 mCi ^{57}Co source in a Rh matrix. The velocity scale was calibrated using α-Fe foil. Isomer shifts, IS, are given relative to this standard at room temperature. The absorbers were obtained by packing the powdered samples into perspex holders. Absorber thicknesses were calculated on the basis of the corresponding electronic mass-absorption coefficients for the 14.4 keV radiation, according to G. J. Long *et al.*[19] The spectra were fitted to Lorentzian lines.[20] The relative areas and widths of both peaks in a quadrupole doublet were kept equal during refinement.

Results and discussion

Synthetic approach and stability in aqueous solution

Reaction of the potassium salts of $[Fe(C_2O_4)_3]^{3-}$ or $[Fe(C_3H_2O_4)_3]^{3-}$ with the trivacant POM $[A\text{-}\alpha\text{-}PW_9O_{34}]^{9-}$ in aqueous solution at 60 °C results in the crystallization of the sandwich-type molecular complexes **1** and **2** which contain two iron atoms, each one coordinated by one oxalato ligand in **1** (or malonato for **2**) and two $[A\text{-}\alpha\text{-}PW_9O_{34}]^{9-}$ moieties. The formation of **1** and **2** takes place owing to the lability of the tris(oxalato) and tris(malonato)ferrate(III) complexes, which quickly and readily exchange two dicarboxylate ligands by two $[A\text{-}\alpha\text{-}PW_9O_{34}]^{9-}$ moieties (substitution of the three dicarboxylate ligands is not possible due to the steric effect imposed by the bulky $[A\text{-}\alpha\text{-}PW_9O_{34}]^{9-}$ anion). This is consistent with the impossibility of obtaining analogous POMs containing Cr or Ru using the same reaction conditions as for **1**, *i.e.* using the more kinetically inert tris(oxalato)chromate(III) or tris(oxalato)ruthenate(III) complexes. On the other hand, the reaction of $[A\text{-}\alpha\text{-}PW_9O_{34}]^{9-}$ with the kinetically labile $[Co(C_2O_4)_3]^{3-}$ or $[Mn(C_2O_4)_3]^{3-}$ does not give the analogous POMs of **1** containing Co(III) or Mn(III) due to their strong oxidizing character in aqueous solution.

The crystal structures of **1** and **2** (see below) reveal that both POMs enclose a potassium ion in their internal cavity. It seems that K^+ ions act as templates for the assembly of two $[A\text{-}\alpha\text{-}PW_9O_{34}]^{9-}$ and two $Fe(C_2O_4)^+$ (or $Fe(C_3H_2O_4)^+$) moieties to form **1** and **2**. We have attempted unsuccessfully to enclose other alkaline ions (Na^+, for example) in the central cavity of these POMs. Hence, the presence of K^+ ions in the reaction medium seems to be essential for the formation of **1** and **2**. This is attributed to the rigidity of the POM, which has a cavity size only suitable to accommodate potassium.

The stability in aqueous solution of **1** and **2** has been studied by UV spectroscopy (Fig. S9†). Both compounds display similar absorption bands in the range 190–400 nm: **1** exhibits a shoulder at 201 nm (204 nm for **2**) and a band centred at 257 nm (258 nm for **2**). The absorption at higher energy is due to the $p\pi$–$d\pi$ charge-transfer transitions of the $O_t \rightarrow W$ in the polyoxoanion (O_t: terminal oxygen), while the lower energy band can be assigned to the $p\pi$–$d\pi$ charge transfer transitions of $O_{b,c} \rightarrow W$ in the polyoxoanion[21] ($O_{b,c}$ = bridging oxygen). The evolution of the UV spectra over 24 h reveals that the positions of the absorption bands do not change with time, but they become less intense over time, pointing to a slow

decomposition of both compounds in aqueous solution at room temperature. The compounds, however, can be recrystallized from aqueous solution if the process is carried out within a short time using concentrated solutions of **1** or **2** (∼30 min).

Crystal structures

The X-ray structures of **1** and **2** reveal that both POMs contain two $[A\text{-}\alpha\text{-}PW_9O_{34}]^{9-}$ moieties, two iron ions, two oxalato (for **1**) or malonato (for **2**) ligands, and one potassium cation encapsulated in the central cavity of each POM (Fig. 1). The two iron ions are sandwiched between the trivacant $[A\text{-}\alpha\text{-}PW_9O_{34}]^{9-}$ anions in such a way that each iron atom is coordinated by two oxygen atoms from two edge-sharing tungsten atoms of each trivacant unit, while the two remaining coordination sites are occupied by one chelating oxalato or malonato ligand.

There are many reported examples of sandwich POMs trapping two or more metal ions between two $[A\text{-}\alpha\text{-}PW_9O_{34}]^{9-}$ ligands.[23] However, regarding first row 3d-transition metals, the most representative series is $[(A\text{-}\alpha\text{-}PW_9O_{34})_2(M(H_2O)_2)_3]^{n-}$ (M^{II} = Mn, Fe, Co, Ni, Cu, Zn, and M^{III} = Fe).[23a–c] The reason why **1** and **2** enclose only two iron atoms and not more lies in the presence of the chelating oxalato or malonato ligands, which occupy two *cis* positions in the octahedral coordination sphere of the metal ions. This forces the two $[A\text{-}\alpha\text{-}PW_9O_{34}]^{9-}$ units to be slightly side-slipped in order to occupy the other four positions of the octahedral coordination spheres of the iron ions (Fig. 2), as a result giving the impossibility of sandwiching a third iron ion. In the previously reported POM compounds enclosing three octahedrally-coordinated 3d transition metal ions, the absence of a chelating ligand (other than $[A\text{-}\alpha\text{-}PW_9O_{34}]^{9-}$) allowed the two trivacant units to be placed directly over each other, leaving the remaining *trans* coordination positions to be occupied by non-chelating ligands.

Therefore, the described arrangement of ligands and metal ions in **1** and **2** would give rise to an overall, idealized C_{2h} symmetry (in which the binary axis passes through the two iron atoms). However, the mean planes of the dicarboxylate ligands are tilted in opposite directions with respect to the mean plane
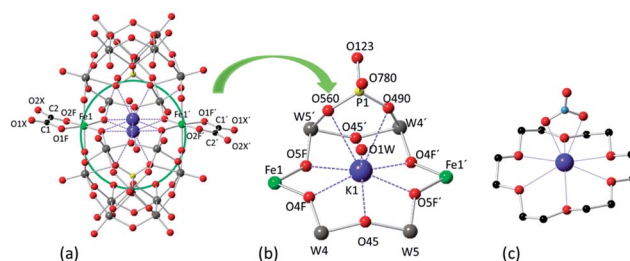

Fig. 1 (a) Ball and stick representation of POM **1**, showing the disorder of the encapsulated potassium ion in the central cavity of the POM. (b) Detailed view of the coordination of the encapsulated potassium ion (the disorder is not shown). (c) Ball and stick representation showing the coordination of potassium by 18-crown-6 and nitrate in [K⊂(18-crown-6)](NO₃)(HNO₃).[22] The colour code of the spheres is as follows: W (grey), Fe (green), K (violet), P (yellow), O (red) and C (black). K···O coordination contacts are shown as dotted lines.

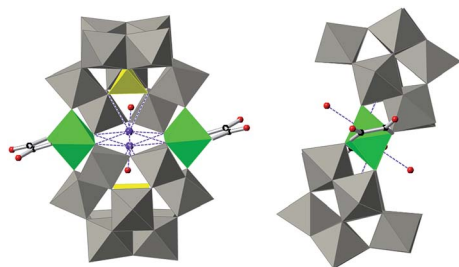**Fig. 2** Combined polyhedral/ball-and-stick representations of the POM in **1**. Gray octahedra, [WO₆]; yellow tetrahedra, [PO₄]; green octahedra, [FeO₆]; black spheres, C; red spheres, O.

formed by the Fe atom and the equatorial O ligands by 18.7(9)° and 22.9(5)° for **1** and **2**, respectively (see Fig. 2),‡ reducing the overall symmetry of the POM from C_{2h} to C_i. Bond valence sum calculations[24] suggest an oxidation state of +3 for the iron ions in **1** and **2** (this is confirmed by Mössbauer and magnetic measurements, see below and the ESI†) and that all O atoms in the POMs are non-protonated (see Fig. S5†).

The side-slipped arrangement of the two $[A-\alpha-PW_9O_{34}]^{9-}$ moieties creates an internal cavity in the centre of POMs **1** and **2** which is occupied by a nine-coordinated potassium cation. This internal cavity can be considered as an oxygen pocket formed by an equatorial ring of six μ₂-O atoms of the POM (O4F, O5F, O45, O4F′, O5F′ and O45′) which has a chair-like arrangement about the potassium ion, and four other μ₃-O atoms of the POM (O490, O560, O490′, O560′), two at each opposite side of the equatorial ring. The six μ₂-O atoms either bridge two W atoms (O45 and O45′) or W and Fe atoms (O4F, O5F, O4F′ and O5F′), while the four μ₃-O atoms bridge one P and two W atoms. The potassium ion is enclosed in the centre of this oxygen pocket although it is disordered over two equivalent and close positions separated by 1.11 Å (or 1.02 Å) in **1** (or **2**). This disorder enables K⁺ to be coordinated by two of the μ₃-O atoms located on one side of the equatorial ring made of the six μ₂-O atoms. K⋯μ₂-O distances range from 2.595(19) to 2.868(19) Å for **1** (2.559(6) to 2.834(6) Å for **2**) and K⋯μ₃-O distances are 2.917(19) and 2.943(16) Å in **1** (2.924(6) and 2.957(6) Å in **2**). A water molecule completes the ninth coordination of the K⁺ ion with a K⋯O_w distance of 2.72(3) Å for **1** (2.783(10) Å for **2**). This situation is strongly reminiscent of the typical potassium complexes of the 18-crown-6 polyether ligand.[25] The rigidity of the internal cavity created by the POM, however, makes it much more selective to K⁺ coordination than the flexible organic 18-crown-6 polyether, which can also coordinate other smaller or larger alkaline cations.[25]

Photocoloration effect

When a solid sample of **1** is exposed to direct sunlight or UV irradiation, a colour change from light yellowish-green to black, visible by the naked eye, starts in a matter of seconds (Fig. 3). If this black solid is stored in the dark in the presence of air, the solid reverts to its original colour after about 7 days (no colour reversion takes place under an O₂-free atmosphere).

UV-vis/diffuse absorbance spectra of **1**, before and after irradiation with UV light (351 nm) during different irradiation times, are shown in Fig. 4. Before UV irradiation, the sample exhibits two absorption bands in the visible region; a weak, broad absorption band centred at 630 nm and a narrower and stronger band at 460 nm. In addition there are two broad, significant bands at lower wavelengths (ranging between 210–270 and 320–370 nm) attributed to O → W ligand to metal charge transfer (LMCT) bands of the POM (Fig. 4, inset).

After irradiation, the colour of the sample turns black, in agreement with the growth of the two absorption bands in the visible range. The broader band in this region is quite comparable with those of other irradiated photochromic POMs,[6d,e,26] suggesting that the photoinduced coloration is mainly due to the POM core. This should imply that in **1** the two POM moieties have been reduced as a result of the UV irradiation and contain W(v) species. Therefore, the absorption in the visible range can be attributed to d–d transitions (if the electron is trapped onto a specific W centre) or intervalence charge transfer (IVCT) of W(v) → W(vi) (if it can be delocalized onto several adjacent {WO₆}). In addition, the position of the maximum absorption of the broader band undergoes a blue shift with irradiation time from 630 nm to about 550 nm, suggesting that the degree of reduction in the POMs increases with irradiation time. After the UV irradiation was stopped, the sample was stored in the dark at room temperature in the presence of air. Under these conditions, the sample slowly reverts to its original colour. After 7 days, the absorption spectrum is very similar to the original one (dotted line in Fig. 4) meaning that W(v) is reoxidised to W(vi) in the presence of air. The coloration and bleaching process can be repeated at least 6 times if the sample is exposed again to UV light, although the intensity of the black colour decreases after each cycle. In contrast, **2** does not exhibit any light-induced colour change under similar conditions, as shown by its UV-vis/diffuse absorbance spectra (Fig. S12†).

The coloration kinetics of **1** have been quantified by analysing its reflectivity values, $R(t)$, in the range of 380–800 nm
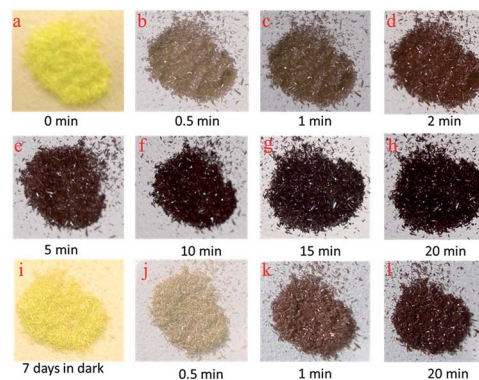

Fig. 3 (a–h) Photogenerated colour change of **1** after different UV irradiation times at 351 nm (0–20 min). After being irradiated, the compound was stored in the dark for 7 days (i) and then re-irradiated again (j–l). Photographs of individual irradiated crystals of **1** are shown in the ESI (Fig. S13 and S14†).
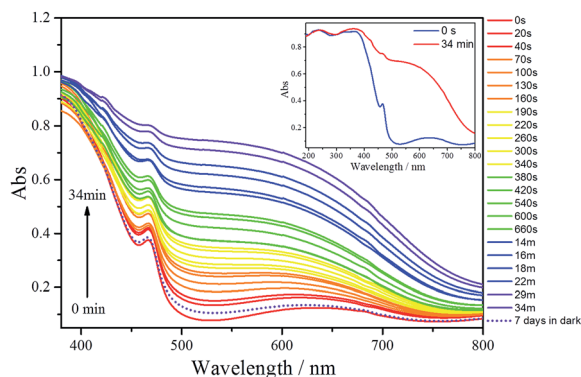
Fig. 4 Evolution of the photogenerated absorption of **1** after 0, 0.17, 0.67, 1.17, 1.67, 2.17, 2.67, 3.17, 3.67, 4.33, 5, 5.67, 6.33, 9, 10, 11, 14, 16, 18, 22, 29 and 34 min of UV irradiation (351 nm). After being irradiated for 34 min, the compound was stored in the dark for 7 days and its absorption spectrum recorded (dotted line). Inset: UV-vis/diffuse absorbance spectra of **1** (before UV irradiation and after 34 min of UV irradiation) in the 190–800 nm range.

as a function of irradiation time, t (Fig. S10†). Details of the parameters related to the coloration kinetics are given in the ESI (Table S3†). In summary, it has been found that the $R^{525}(t)$ vs. t curves of **1** can be fitted using the pseudo-second order law $R^{525}(t) = a/[bt + 1] + [R^{525}(0) - a]$ (Fig. S11†). The $t_{1/2}$ value obtained for the photocoloration process (4.25 min) corresponds to a relatively fast photoresponse compared to other POM-based photochromic materials.[26c,27]

Infrared spectroscopy

The IR spectra of **1** (as a KBr pressed pellet) before and after UV photoirradiation were investigated (Fig. 5). Before irradiation it exhibits the typical bands of the chelating oxalato ligand[28] at 1714 cm^{-1} (ν_a(C=O), very weak), 1668 cm^{-1} (ν_a(C=O), strong), 1384 and 1401 cm^{-1} (ν_s(CO) + ν(CC), strong) and 1285 cm^{-1} (ν_s(CO) + δ(O–C=O), medium), and bands corresponding to the POM framework at 1076 and 1018 cm^{-1} (ν_a(P–O), strong), 940 cm^{-1} (ν_a(W–O$_t$), strong), 852 and 800 cm^{-1} (ν_a(W–O$_a$–W), strong) and 742 cm^{-1} (ν_a(W–O$_b$–W), strong). Bands at 659 and 519 cm^{-1} can be assigned to Fe–O–W and Fe–O–C vibrations.
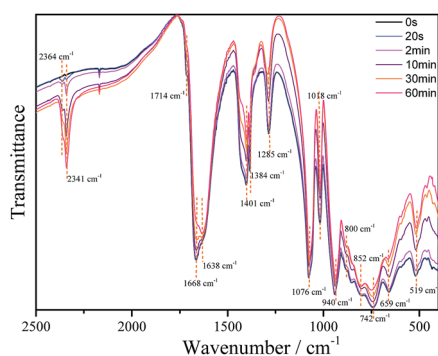

Fig. 5 Evolution of the IR spectra of **1** upon different irradiation times of UV light (351 nm).

Upon irradiation, the intensity of all oxalato bands decreases gradually as the irradiation time increases, while there are two new bands that appear and increase in intensity with irradiation time, at 2341 and 2364 cm^{-1}. These bands can be attributed to carbon dioxide (R- and P-branches of the ν_a(CO$_2$) band, respectively) trapped in the KBr pellet.[29]

These results confirm a photoinduced decomposition of the oxalato ligand into carbon dioxide, akin to the photodecomposition of the oxalato ligands in the tris(oxalato)ferrate(III) complex anion.[30] During this process, two electrons must be released from each oxalato ligand that decomposes, which may be accepted by the POM framework and/or the iron atoms. The decrease in the intensity of all the POM bands upon irradiation is consistent with a reduction of the POM.[26a]

XPS spectra

The XPS W4f spectra collected for **1** before irradiation, after UV irradiation, and after being stored in the dark during 7 days are shown in Fig. 6. All three XPS W4f spectra can be resolved into 4f$_{7/2}$ and 4f$_{5/2}$ doublets (caused by spin–orbit coupling) and deconvoluted into two couples of peaks (Fig. 6a–c), corresponding to the typical binding energies of W(VI) (centred at 37.9 and 35.7 eV) and W(V) oxidation states (centred at 37.0 and 34.9 eV). As shown in Table 1, W(V) species appear even in the non-irradiated sample (Fig. 6a), suggesting that the photoreduction of the POM occurs in part when the sample is exposed to an X-ray source, as observed in other previously published work.[26d,31] Data analysis indicates that after photoirradiation with 351 nm UV light for 3 days under vacuum, the amount of W(V) increases and the amount of W(VI) decreases (Fig. 6b). The concentration of W(V) is 11.0% (Table 1), as determined from the peak area ratio of W(V) to W(VI) (much higher than that observed before irradiation), indicating the reduction of more W(VI) to W(V) under UV irradiation.

The XPS spectrum of the photoirradiated sample stored in dark (Fig. 6c) exhibits very similar binding energies of the W4f peaks to those of the non-irradiated sample, and can be deconvoluted into one pair of peaks that corresponds to the typical binding energies of W(VI) (centred at 37.9 and 35.7 eV). The concentration of W(V) in these two samples is also very similar (4.0% compared to 3.0% for the irradiated and the initial samples, respectively).

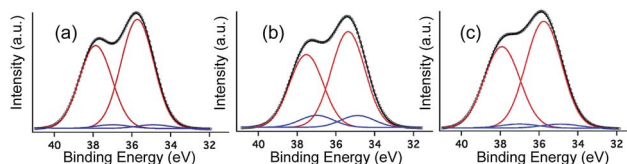**Fig. 6** XPS W4f spectra collected for **1** before irradiation (a), after 3 days of UV irradiation (351 nm) (b) and 7 days more in the dark (c). Dotted lines correspond to the experimental data that can be deconvoluted into two pairs of peaks corresponding to W(VI) (red curves) and W(V) (blue curves). Fitting of the experimental data (black curves) has been obtained by summation of the deconvoluted peaks.

Table 1 XPS data of **1** before irradiation, 3 days UV irradiation (351 nm) under vacuum and 7 days in the dark in air

Species		Before irradiation		After irradiation		7 days in the dark	
		Peak, BE/eV	W(v)%	Peak, BE/eV	W(v)%	Peak, BE/eV	W(v)%
W4f	W(vi)4f$_{5/2}$	35.7	3.0%	35.4	11.0%	35.7	4.0%
	W(vi)4f$_{7/2}$	37.9		37.5		37.9	
	W(v)4f$_{5/2}$	34.9		34.9		34.9	
	W(v)4f$_{7/2}$	37.0		37.0		37.0	

Mössbauer spectroscopy

The Mössbauer spectra of **1-^{57}Fe** and **2-^{57}Fe** consist of a broad absorption peak (Fig. 7a and S15†), which may be fitted by a quadrupole doublet. Only a broad peak is observed in both spectra because the widths of each line of the doublets are higher than the corresponding quadrupole splittings, QS (Table S4†). The isomer shifts relative to α-Fe at 295 K, IS, are within the range of high spin, $S = 5/2$, Fe(iii) values[32] and similar to those of Fe(iii) coordinated to oxalato or malonato ligands in other compounds.[20,33]
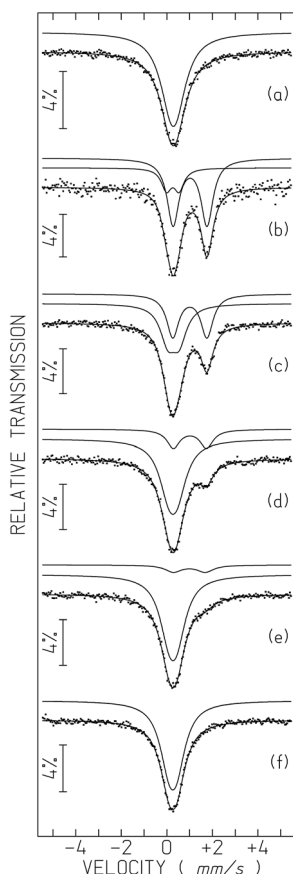

Fig. 7 Mössbauer spectra of **1-^{57}Fe** sample taken before (a) and after 6 h UV irradiation for $t_{UV} \sim 0.75$ h (b), 18 h (c), 42 h (d), 66 h (e) and 12 days (f). t_{UV}, time after irradiation was switched off, is defined in the text. The lines over the experimental points are the sum of two quadrupole doublets shown slightly shifted for clarity (estimated parameters in Table S4†).

After irradiation by UV light (365 nm) the **1-^{57}Fe** sample changes colour from light yellowish-green to almost black. After 6 h irradiation time the sample was moved to the Mössbauer spectrometer. At least 45 minutes of data collection was necessary for a reliable analysis (Fig. 7b). The spectrum obtained can only be analysed by two quadrupole doublets. One of the doublets has an IS (Table S4†) typical of high-spin Fe(ii), $(S = 2)$,[20,32,34] far above the range of the Fe(iii) IS values. The second doublet is similar to the Fe(iii) signal in the pristine sample but with a higher QS, most likely due to a more distorted Fe(iii) environment in the UV-irradiated sample.

Both high-spin Fe(iii) and Fe(ii) doublets are present in the spectra taken at different times after UV-irradiation (up to 10 days). The relative area of Fe(ii) and I(Fe^{II}) decreases with increasing time after irradiation (Fig. 7 and S16†). In order to evidence the time dependence of I(Fe^{II}), all spectra except for the first one after irradiation, were collected during approximately the same time and t_{UV} was defined as the time elapsed between mid-spectrum collection and the moment when UV irradiation was switched off (which corresponds to $t_{UV} = 0$). The relative areas estimated for $t_{UV} = 0.75$ hours suggest that approximately 79% of all the Fe is in the 2+ oxidation state, i.e. I(Fe^{II}) $\sim$79%. The steep decrease of I(Fe^{II}) with increasing t_{UV} during the first hours (Table S4, Fig. S16†) suggests that the I(Fe^{II}) deduced from the spectra are actually an average of the I(Fe^{II}) range of values occurring during the spectrum collection time. This means that immediately after UV irradiation I(Fe^{II}) is most likely higher than 79%.

When $t_{UV} \sim 66$ hours, I(Fe^{II}) reaches 11% $\pm$ 2%, but at this stage it decreases very slowly with increasing time. After approximately 10 days the colour of the sample becomes light yellowish-green again but a small shoulder on the Fe(iii) absorption peak evidences the presence of an Fe(ii) doublet with an estimated I(Fe^{II}) $\sim$4%. Only after 12 days do all traces of Fe(ii) disappear from the spectrum (Fig. 7f and S16, Table S4†).

The IS of Fe(iii) is consistent with octahedral coordination, in agreement with the structure determined by single-crystal XRD for the pristine compound. The IS of Fe(ii) is also consistent with octahedral coordination but the presence of a fraction of Fe(ii) in lower coordination, such as penta-coordination, may not be excluded.[32,35]

The effect of a second UV irradiation of the sample after all Fe returns to the +3 oxidation state, is not the same as the effect of the first irradiation. The sample colour resulting from this second irradiation is not so dark and the Mössbauer spectra

(Fig. S17†) taken for similar t_{UV} reveal that I(Fe^{II}) is significantly lower in the first days after irradiation (Table S4, Fig. 7, S16 and S17†). The estimated I(Fe^{II}) for the spectrum taken during 45 minutes immediately after turning off the UV light is only ~20%. After 12 days all the Fe is back in the +3 oxidation state.

The IS and the QS of Fe(II) obtained after the second irradiation are significantly different (the IS is smaller and the QS is higher) from those obtained after the first irradiation. The lower IS may be explained if we assume that after the second irradiation Fe(II) is mainly pentacoordinated.[32,35] This coordination of Fe(II) would also lead to a more distorted electronic charge distribution around the Fe(II) in agreement with a higher QS.

As mentioned above, the QS of Fe(III) increases significantly after the first UV-irradiation, suggesting a more distorted environment of this cation. However, as I(Fe^{II}) decreases, QS of Fe(III) also decreases, until it becomes slightly lower than in the pristine sample where I(Fe^{II}) is zero. This may suggest that by the end of the first "UV-irradiation-Fe(II) decay" cycle the structure of the sample is no longer identical to the pristine one although all the Fe is in the same oxidation state, +3, and apparently has the same coordination number, 6. Only the ligands of Fe(III) and/or their geometrical arrangement seem to be different. Such a structural modification would be related to the distinct behaviour during the second UV-irradiation, rendering the sample more reluctant to Fe(III) reduction. In summary, Mössbauer spectroscopy clearly shows that UV-irradiation induces a Fe(III) reduction to Fe(II). The variation of hyperfine parameters also suggests structural modifications after the first cycle of UV irradiation and Fe(II) decay back to Fe(III).

## Mechanism of the photoinduced coloration and final discussion

In this section we gather the experimental results described in the previous sections with the objective of proposing a mechanism for the photoinduced coloration of **1**. When exposed to UV irradiation, the light yellowish-green solid samples of **1** become black in a fast photocoloration process having a $t_{1/2}$ value of 4.25 min (as indicated by UV-vis/DRS measurements), while **2** does not exhibit any photoinduced colour change. IR spectroscopy clearly indicates that the UV irradiation initiates a photodecomposition of the oxalato ligands of **1** into CO_2. This is confirmed by carbon analysis results, which indicate that there is a lesser amount of carbon in the irradiated compound than in the initial one (0.49% vs. 0.81%). Each oxalato ligand that decomposes into CO_2 releases two electrons, which presumably are transferred to the iron and/or tungsten atoms of the POM. The DRS measurements suggest that photocoloration is due to the photoreduction of W(VI) ($5d^0$) to W(V) ($5d^1$) and occurs via d–d transitions and/or W(VI)/W(V) intervalence charge transfer in the POM core; XPS measurements confirm the presence of up to 11.0% W(V) in the irradiated compound. On the other hand, Mössbauer measurements confirm the presence of Fe(II) (79%) in the irradiated samples of **1**-^{57}Fe and discard it in non-irradiated samples. The magnetic properties of non-irradiated and irradiated samples of **1** are compatible with this scenario (see the ESI†).

In view of all the experimental evidence, the photocoloration effect in **1** could arise according to the mechanism proposed in Scheme 3. UV irradiation induces the photodissociation of the coordinated bond between Fe(III) and the oxalato ligand, resulting in a ligand-to-metal charge transfer that yields Fe(II) and a carbon dioxide radical ion ($CO_2^{\cdot-}$). Concomitantly, the radical ion most likely reacts with the POM yielding reduced W(V) ions, responsible for the intense photocoloration of **1**.

According to the carbon analysis results and the TGA curve of an irradiated sample of **1** (see Fig. S4†), it is possible to deduce the formula $K_{16}[(PW_9O_{34})_2Fe_2(C_2O_4)_x] \cdot nH_2O$ (x = 1.16 and n = 20.6), which clearly reflects the partial loss of oxalato ligands under these conditions of UV irradiation (the decrease in the number of water molecules of crystallization is due to the vacuum conditions employed during the irradiation process). This formula must be regarded in compositional terms only, as it does not reflect either the possible structural modifications of the trivacant $[A-\alpha-PW_9O_{34}]^{9-}$ moieties or the change in coordination environment of the Fe atoms that almost certainly happens after the photodecomposition of the oxalato ligands and concomitant reduction of the Fe atoms and POM core (powder diffraction indicates that solid samples of **1** tend to amorphise upon irradiation, see Fig. S8†).

If this irradiated black solid is stored in the dark in the presence of air, it reverts to its original light yellowish-green colour after about 7 days (DRS measurements show that the absorbance of a reversed sample is almost the same as that before irradiation). As no colour reversion takes place under an O_2-free atmosphere, it must be assumed that O_2 is able to oxidize the W(V) back to W(VI). This is confirmed by XPS measurements of a reversed sample, which indicates that the concentration of W(V) is similar to the value found in the initial, non-irradiated sample. Moreover, Mössbauer measurements indicate also that the Fe(II) ions are oxidized back to Fe(III) after keeping the irradiated samples for 12 days in the dark in the presence of air.

Finally, the process of photoinduced coloration and colour reversion in the presence of air can be repeated at least 6 times for the same sample, although the photoinduced coloration is less intense after every cycle (the fading time keeps approximately constant after each cycle (~7 days)). This could be anticipated because less amounts of oxalato ligands are expected in the sample after each cycle of UV irradiation. Although the decrease of oxalato ligands after the second
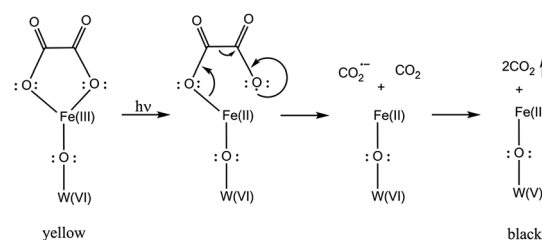
Scheme 3 The mechanism depicted here implies a W atom directly connected (through an oxo bridge) to a Fe atom, but can be transposable to other W atoms.

irradiation could not be confirmed by carbon analysis (the low percentage of C in the reirradiated samples gave non-reproducible values), it is consistent with the Mössbauer results, which show that a much lower concentration of Fe(II) is attained after the irradiation of a reversed sample with UV light, under the same conditions as the irradiation of the pristine sample (20% after the second irradiation *vs.* 79% after the first irradiation).

In conclusion, **1** represents a new photoresponsive POM-based system that exhibits a remarkable photocoloration effect (from light yellowish-green to black) in the solid state when irradiated with UV light due to the partial photodecomposition of oxalato ligands and release of CO_2, concomitant with a partial reduction of W(VI) and Fe(III) to W(V) and Fe(II). As the photocoloration effect can be repeated several times, this result opens the possibility of obtaining new POM-based materials that incorporate other photoactive Fe(III) carboxylate moieties, which would give rise to different photoresponsive systems with tuneable properties. In addition, we are currently studying the deposition of **1** on different substrates to test its use as chemical actinometer in the solid state. The most widely accepted actinometer is the tris(oxalato)ferrate(III) complex (also called ferrioxalate), due to its wide wavelength range of absorption and high quantum yield.[10] Thanks to the POM, **1** exhibits a high contrast photocoloration effect, which is advantageous for its use in solid state actinometry without the need of a post irradiation analytical procedure. Notice that in the standard ferrioxalate actinometry, phenanthroline is needed as a complexation reagent for Fe(II) and subsequent colour development. In our case, this may enable the *in situ* quantification of the light intensity in a simpler way by monitoring the absorbance of the irradiated solid sample of **1**.

Acknowledgements

Notes and references

‡ All six atoms of the oxalato ligand are used to calculate the mean plane, while only the coordinated oxygen atoms and the sp^2 carbon atoms of the malonato ligand are used to calculate the mean plane.

1 (*a*) E. Coronado and G. Mínguez Espallargas, *Chem. Soc. Rev.*, 2013, **42**, 1525–1539, DOI: 10.1039/C2CS35278H; (*b*) S. Biswas, P. Kumari, P. M. Lakhani and B. Ghosh, *Eur. J. Pharm. Sci.*, 2016, **83**, 184–202, DOI: 10.1016/j.ejps.2015.12.031; (*c*) E. Cariati, E. Lucenti, C. Botta, U. Giovanella, D. Marinotto and S. Righetto, *Coord. Chem. Rev.*, 2016, **306**, 566–614, DOI: 10.1016/j.ccr.2015.03.004; (*d*) H. Chen, D. Liu and Z. Guo, *Chem. Lett.*, 2016, **45**, 242–249, DOI: 10.1246/cl.151176; (*e*) M. Karimi, A. Ghasemi, P. Sahandi Zangabad, R. Rahighi, S. M. Moosavi Basri, H. Mirshekari, M. Amiri, Z. Shafaei Pishabad, A. Aslani, M. Bozorgomid, D. Ghosh, A. Beyzavi, A. Vaseghi, A. R. Aref, L. Haghani, S. Bahrami and M. R. Hamblin, *Chem. Soc. Rev.*, 2016, **45**, 1457–1501, DOI: 10.1039/c5cs00798d; (*f*) M. Lemanowicz, A. Gierczycki and W. Kuźnik, *Polimery*, 2016, **61**, 92–97, DOI: DOI/10.14314/polimery.2016.092; (*g*) Z. Liu, W. Wang, R. Xie, X. Ju and L. Chu, *Chem. Soc. Rev.*, 2016, **45**, 460–474, DOI: 10.1039/c5cs00692a; (*h*) T. Lu, W. Peng, S. Zhu and D. Zhang, *Nanotechnology*, 2016, **27**, 122001, DOI: 10.1088/0957-4484/27/12/122001; (*i*) C. G. Palivan, R. Goers, A. Najer, X. Zhang, A. Car and W. Meier, *Chem. Soc. Rev.*, 2016, **45**, 377–411, DOI: 10.1039/c5cs00569h; (*j*) H. Wang, Q. Huang, H. Chang, J. Xiao and Y. Cheng, *Biomater. Sci.*, 2016, **4**, 375–390, DOI: 10.1039/c5bm00532a.

2 (*a*) P. Gütlich, Y. García and T. Woike, *Coord. Chem. Rev.*, 2001, **219**, 839–879, DOI: 10.1016/S0010-8545(01)00381-2; (*b*) S. Ohkoshi, H. Tokoro, T. Hozumi, Y. Zhang, K. Hashimoto, C. Mathonière, I. Bord, G. Rombaut, M. Verelst, C. C. D. Moulin and F. Villain, *J. Am. Chem. Soc.*, 2006, **128**, 270–277, DOI: 10.1021/ja0559092; (*c*) S. Ohkoshi and H. Tokoro, *Acc. Chem. Res.*, 2012, **45**, 1749–1758, DOI: 10.1021/ar300068k; (*d*) G. Abellán, E. Coronado, C. Martí-Gastaldo, A. Ribera, J. L. Jordá and H. García, *Adv. Mater.*, 2014, **26**, 4156–4162, DOI: 10.1002/adma.201400713; (*e*) G. Abellán, C. Martí-Gastaldo, A. Ribera and E. Coronado, *Acc. Chem. Res.*, 2015, **48**, 1601–1611, DOI: 10.1021/acs.accounts.5b00033; (*f*) H. Tokoro and S. Ohkoshi, *Bull. Chem. Soc. Jpn.*, 2015, **88**, 227–239, DOI: 10.1246/bcsj.20140264.

3 (*a*) D. Bléger and S. Hecht, *Angew. Chem., Int. Ed.*, 2015, **54**, 11338–11349, DOI: 10.1002/anie.201500628; (*b*) M. Fredersdorf, R. Göstl, A. Kolmer, V. Schmidts, P. Monecke, S. Hecht and C. M. Thiele, *Chem.–Eur. J.*, 2015, **21**, 14545–14554, DOI: 10.1002/chem.201501842; (*c*) W. Wang, J. Hu, M. Zheng, L. Zheng, H. Wang and Y. Zhang, *Org. Biomol. Chem.*, 2015, **13**, 11492–11498, DOI: 10.1039/c5ob01912e; (*d*) M. Han, Y. Luo, B. Damaschke, L. Gómez, X. Ribas, A. Jose, P. Peretzki, M. Seibt and G. H. Clever, *Angew. Chem., Int. Ed.*, 2016, **55**, 445–449, DOI: 10.1002/anie.201508307.

4 (*a*) E. J. Harbron, C. M. Davis, J. K. Campbell, R. M. Allred, M. T. Kovary and N. J. Economou, *J. Phys. Chem. C*, 2009, **113**, 13707–13714, DOI: 10.1021/jp9037864; (*b*) S. Köytepe, M. H. Demirel, A. Gültek and T. Seçkin, *Polym. Int.*, 2014, **63**, 778–787, DOI: 10.1002/pi.4596.

5 (*a*) M. T. Pope, *Heteropoly and Isopoly Oxometalates*, Springer-Verlag Berlin, Heidelberg, 1983; (*b*) M. T. Pope and A. Muller, *Angew. Chem., Int. Ed. Engl.*, 1991, **30**, 34–48, DOI: 10.1002/anie.199100341; (*c*) W. He, S. Li, H. Zang, G. Yang, S. Zhang, Z. Su and Y. Lan, *Coord. Chem. Rev.*, 2014, **279**,

141–160, DOI: 10.1016/j.ccr.2014.03.022; (d) M. Mirzaei, H. Eshtiagh-Hosseini, M. Alipour and A. Frontera, *Coord. Chem. Rev.*, 2014, **275**, 1–18, DOI: 10.1016/j.ccr.2014.03.012; (e) J. J. Walsh, A. M. Bond, R. J. Forster and T. E. Keyes, *Coord. Chem. Rev.*, 2016, **306**, 217–234, DOI: 10.1016/j.ccr.2015.06.016.

6 (a) T. He and J. Yao, *Prog. Mater. Sci.*, 2006, **51**, 810–879, DOI: 10.1016/j.pmatsci.2005.12.001; (b) V. Coué, R. Dessapt, M. Bujoli-Doeuff, M. Evain and S. Jobic, *Inorg. Chem.*, 2007, **46**, 2824–2835, DOI: 10.1021/ic0621502; (c) Y. Yang, L. Yue, H. Li, E. Maher, Y. Li, Y. Wang, L. Wu and V. W. Yam, *Small*, 2012, **8**, 3105–3110, DOI: 10.1002/smll.201200768; (d) H. El Moll, A. Dolbecq, I. M. Mbomekalle, J. Marrot, P. Deniard, R. Dessapt and P. Mialane, *Inorg. Chem.*, 2012, **51**, 2291–2302, DOI: 10.1021/ic202299d; (e) K. Hakouk, O. Oms, A. Dolbecq, H. El Moll, J. Marrot, M. Evain, F. Molton, C. Duboc, P. Deniard, S. Jobic, P. Mialane and R. Dessapt, *Inorg. Chem.*, 2013, **52**, 555–557, DOI: 10.1021/ic302477p; (f) Q. Zheng, L. Vilà-Nadal, C. Busche, J. S. Mathieson, D. Long and L. Cronin, *Angew. Chem., Int. Ed.*, 2015, **54**, 7895–7899, DOI: 10.1002/anie.201502295; (g) Y. Gong, Q. Hu, C. Wang, L. Zang and L. Yu, *Langmuir*, 2016, **32**, 421–427, DOI: 10.1021/acs.langmuir.5b03883; (h) W. Chen, U. Tong, T. Zeng, C. Streb and Y. Song, *J. Mater. Chem. C*, 2015, **3**, 4388–4393, DOI: 10.1039/c5tc00379b; (i) C. Streb, *Dalton Trans.*, 2012, **41**, 1651–1659, DOI: 10.1039/c1dt11220a; (j) B. Matt, J. Fize, J. Moussa, H. Amouri, A. Pereira, V. Artero, G. Izzet and A. Proust, *Energy Environ. Sci.*, 2013, **6**, 1504–1508, DOI: 10.1039/c3ee40352a; (k) A. Proust, R. Thouvenot and P. Gouzerh, *Chem. Commun.*, 2008, 1837–1852, DOI: 10.1039/b715502f; (l) C. Zhao, C. S. Kambara, Y. Yang, A. L. Kaledin, D. G. Musaev, T. Lian and C. L. Hill, *Inorg. Chem.*, 2013, **52**, 671–678, DOI: 10.1021/ic301766b.

7 T. Yamase, *Chem. Rev.*, 1998, **98**, 307–325, DOI: 10.1021/cr9604043.

8 R. Q. Fang, X. M. Zhang, H. S. Wu and S. W. Ng, *Acta Crystallogr., Sect. E: Struct. Rep. Online*, 2004, **60**, M359–M361, DOI: 10.1107/S1600536804004647.

9 L. Deguillaume, M. Leriche, K. Desboeufs, G. Mailhot, C. George and N. Chaumerliac, *Chem. Rev.*, 2005, **105**, 3388–3431, DOI: 10.1021/cr040649c.

10 H. J. Kuhn, S. E. Braslavsky and R. Schmidt, *Pure Appl. Chem.*, 2004, **76**, 2105–2146, DOI: 10.1351/pac200476122105.

11 (a) E. L. Simmons and W. W. Wendlandt, *Coord. Chem. Rev.*, 1971, **7**, 11–27, DOI: 10.1016/S0010-8545(00)80006-5; (b) Y. G. Zuo and J. Hoigne, *Environ. Sci. Technol.*, 1992, **26**, 1014–1022, DOI: 10.1021/es00029a022; (c) B. C. Faust and R. G. Zepp, *Environ. Sci. Technol.*, 1993, **27**, 2517–2522, DOI: 10.1021/es00048a032.

12 (a) A. Dolbecq, J. Compain, P. Mialane, J. Marrot, E. Rivière and F. Sécheresse, *Inorg. Chem.*, 2008, **47**, 3371–3378, DOI: 10.1021/ic7024186; (b) A. Sartorel, M. Carraro, G. Scorrano, B. S. Bassil, M. H. Dickman, B. Keita, L. Nadjo, U. Kortz and M. Bonchio, *Chem.–Eur. J.*, 2009, **15**, 7854–7858, DOI: 10.1002/chem.200901392.

13 (a) R. Contant, *Can. J. Chem.*, 1987, **65**, 568–573, DOI: 10.1139/v87-100; (b) P. J. Domaille and A. P. Ginsberg, *Inorganic Syntheses*, John Wiley & Sons, New York, 1990, pp. 96–104.

14 D. Collison and A. K. Powell, *Inorg. Chem.*, 1990, **29**, 4735–4746, DOI: 10.1021/ic00348a030.

15 Agilent Technologies UK Ltd, Oxford, UK, CrysAlis PRO Software system, 2013.

16 G. M. Sheldrick, *SHELXTL Version, 2014/7*, http://shelx.uni-ac.gwdg.de/SHELX/index.php.

17 R. C. Clark and J. S. Reid, *Acta Crystallogr., Sect. A: Found. Crystallogr.*, 1995, **51**, 887–897, DOI: 10.1107/S0108767395007367.

18 R. H. Blessing, *J. Appl. Crystallogr.*, 1997, **30**, 421–426, DOI: 10.1107/S0021889896014628.

19 G. J. Long, T. E. Cranshaw and G. Longworth, *Moessbauer Eff. Ref. Data J.*, 1983, **6**, 42–49.

20 E. Coronado, J. R. Galán-Mascarós, C. Martí-Gastaldo, J. C. Waerenborgh and P. Gaczyński, *Inorg. Chem.*, 2008, **47**, 6829–6839, DOI: 10.1021/ic800418k.

21 Y. Wang, X. Sun, S. Li, P. Ma, J. Niu and J. Wang, *Cryst. Growth Des.*, 2015, **15**, 2057–2063, DOI: 10.1021/cg5012499.

22 A. N. Chekhlov, *Russ. J. Inorg. Chem.*, 2008, **53**, 928–932, DOI: 10.1134/S0036023608060193.

23 (a) W. H. Knoth, P. J. Domaille and R. D. Farlee, *Organometallics*, 1985, **4**, 62–68, DOI: 10.1021/om00120a012; (b) W. H. Knoth, P. J. Domaille and R. L. Harlow, *Inorg. Chem.*, 1986, **25**, 1577–1584, DOI: 10.1021/ic00230a014; (c) N. M. Okun, T. M. Anderson and C. L. Hill, *J. Am. Chem. Soc.*, 2003, **125**, 3194–3195, DOI: 10.1021/ja0267223; (d) V. Artero, A. Proust, P. Herson, F. Villain, C. C. D. Moulin and P. Gouzerh, *J. Am. Chem. Soc.*, 2003, **125**, 11156–11157, DOI: 10.1021/ja036257p; (e) N. Belai and M. T. Pope, *Chem. Commun.*, 2005, 5760–5762, DOI: 10.1039/b509756h; (f) T. M. Anderson, R. Cao, E. Slonkina, B. Hedman, K. O. Hodgson, K. I. Hardcastle, W. A. Neiwert, S. X. Wu, M. L. Kirk, S. Knottenbelt, E. C. Depperman, B. Keita, L. Nadjo, D. G. Musaev, K. Morokuma and C. L. Hill, *J. Am. Chem. Soc.*, 2005, **127**, 11948–11949, DOI: 10.1021/ja054131h; (g) R. Villanneau, S. Renaudineau, P. Herson, K. Boubekeur, R. Thouvenot and A. Proust, *Eur. J. Inorg. Chem.*, 2009, 479–488, DOI: 10.1002/ejic.200800727; (h) L. F. Piedra-Garza, M. H. Dickman, O. Moldovan, H. J. Breunig and U. Kortz, *Inorg. Chem.*, 2009, **48**, 411–413, DOI: 10.1021/ic8021694; (i) Y. Saku, Y. Sakai, A. Shinohara, K. Hayashi, S. Yoshida, C. N. Kato, K. Yozac and K. Nomiya, *Dalton Trans.*, 2009, 805–813, DOI: 10.1039/b813710m; (j) R. Cao, K. P. O'Halloran, D. A. Hillesheim, K. I. Hardcastle and C. L. Hill, *CrystEngComm*, 2010, **12**, 1518–1525, DOI: 10.1039/b919934a; (k) C. N. Kato, Y. Katayama, M. Nagami, M. Kato and M. Yamasaki, *Dalton Trans.*, 2010, **39**, 11469–11474, DOI: 10.1039/c0dt00722f; (l) G. Wang, C. Pan, K. Li, X. Cui, H. Wang, Y. Wang, S. Shi and J. Xu, *Inorg. Chem. Commun.*, 2010, **13**, 116–118, DOI: 10.1016/j.inoche.2009.10.034; (m) R. Villanneau, D. Racimor, E. Messner-Henning, H. Rousselière, S. Picart,

R. Thouvenot and A. Proust, *Inorg. Chem.*, 2011, **50**, 1164–1166, DOI: 10.1021/ic102223w; (*n*) D. Zhao and R. Ye, *J. Cluster Sci.*, 2011, **22**, 563–571, DOI: 10.1007/s10876-011-0397-z; (*o*) R. Cao, K. P. O'Halloran, D. A. Hillesheim, S. Lense, K. I. Hardcastle and C. L. Hill, *CrystEngComm*, 2011, **13**, 738–740, DOI: 10.1039/c0ce00828a; (*p*) M. Barsukova-Stuckart, L. F. Piedra-Garza, B. Gautam, G. Alfaro-Espinoza, N. V. Izarova, A. Banerjee, B. S. Bassil, M. S. Ullrich, H. J. Breunig, C. Silvestru and U. Kortz, *Inorg. Chem.*, 2012, **51**, 12015–12022, DOI: 10.1021/ic301892s; (*q*) H. Yang, L. Zhang, L. Yang, X. Zhang, W. You and Z. Zhu, *Inorg. Chem. Commun.*, 2013, **29**, 33–36, DOI: 10.1016/j.inoche.2012.12.011; (*r*) R. Villanneau, A. Ben Djamaa, L. Chamoreau, G. Gontard and A. Proust, *Eur. J. Inorg. Chem.*, 2013, 1815–1820, DOI: 10.1002/ejic.201201257; (*s*) R. Al-Oweini, B. S. Bassil, T. Palden, B. Keita, Y. Lan, A. K. Powell and U. Kortz, *Polyhedron*, 2013, **52**, 461–466, DOI: 10.1016/j.poly.2012.08.050; (*t*) J. M. Berg, A. J. Gaunt, I. May, A. L. Pugmire, S. D. Reilly, B. L. Scott and M. P. Wilkerson, *Inorg. Chem.*, 2015, **54**, 4192–4199, DOI: 10.1021/ic5024345.

24 I. D. Brown and D. Altermatt, *Acta Crystallogr., Sect. B: Struct. Sci.*, 1985, **41**, 244–247, DOI: 10.1107/S0108768185002063.

25 J. W. Steed, *Coord. Chem. Rev.*, 2001, **215**, 171–221, DOI: 10.1016/S0010-8545(01)00317-4.

26 (*a*) X. A. Zhang, W. J. Wu, Y. H. Man, T. Tian, X. Z Tian and J. F. Wang, *Sci. China, Ser. B: Chem.*, 2007, **50**, 318–326, DOI: 10.1007/s11426-007-0038-4; (*b*) L. Zhang, W. Gu, X. Liu, Z. Dong and B. Li, *CrystEngComm*, 2008, **10**, 652–654, DOI: 10.1039/b718523e; (*c*) J. Compain, P. Deniard, R. Dessapt, A. Dolbecq, O. Oms, F. Sécheresse, J. Marrot and P. Mialane, *Chem. Commun.*, 2010, **46**, 7733–7735, DOI: 10.1039/c0cc02533j; (*d*) X. Luo and C. Yang, *Phys. Chem. Chem. Phys.*, 2011, **13**, 7892–7902, DOI: 10.1039/c0cp02243h.

27 R. Dessapt, M. Collet, V. Coué, M. Bujoli-Doeuff, S. Jobic, C. Lee and M. Whangbo, *Inorg. Chem.*, 2009, **48**, 574–580, DOI: 10.1021/ic8013865.

28 K. Nakamoto, Infrared and Raman Spectra of Inorganic and Coordination Compounds. Part B: Applications in Coordination, *Organometallic and Bioinorganic Chemistry*, John Wiley & Sons, 2009.

29 G. Keresztury, M. Incze, F. Sóti and L. Imre, *Spectrochim. Acta, Part A*, 1980, **36**, 1007–1008, DOI: 10.1016/0584-8539(80)80181-4.

30 (*a*) A. S. Brar and B. S. Randhawa, *Bull. Chem. Soc. Jpn.*, 1981, **54**, 3166–3169, DOI: 10.1246/bcsj.54.3166; (*b*) B. S. Randhawa, *J. Radioanal. Nucl. Chem.*, 1998, **230**, 295–298, DOI: 10.1007/BF02387484.

31 W. Feng, Y. S. Ding, Y. Liu and R. Lu, *Mater. Chem. Phys.*, 2006, **98**, 347–352, DOI: 10.1016/j.matchemphys.2005.09.037.

32 N. N. Greenwood and T. C. Gibb, *Mössbauer Spectroscopy*, Chapman and Hall, London, 1971.

33 P. S. Bassi, B. S. Randhawa and S. Kaur, *Hyperfine Interact.*, 1986, **28**, 745–748, DOI: 10.1007/BF02061553.

34 E. Coronado, J. R. Galán-Mascarós, C. J. Gómez-García, J. M. Martínez-Agudo, E. Martínez-Ferrero, J. C. Waerenborgh and M. Almeida, *J. Solid State Chem.*, 2001, **159**, 391–402, DOI: 10.1006/jssc.2001.9169.

35 F. Menil, *J. Phys. Chem. Solids*, 1985, **46**, 763–789, DOI: 10.1016/0022-3697(85)90001-0.